Soft Matter

Accepted Manuscript

ROYAL SOCIETY OF CHEMISTRY

www.rsc.org/softmatter

Soft Matter

RSCPublishing

ARTICLE

Topology Optimization for the Design of Folding Liquid Crystal Elastomer Actuators

Cite this: DOI: 10.1039/x0xx00000x

Kazuko Fuchi[*ac], Taylor H. Ware[*bde], Philip R. Buskohl[b], Gregory W. Reich[a], Richard A. Vaia[b], Timothy J. White[b] and James J. Joo[+a]

Submitted 7th July 2015

DOI: 10.1039/x0xx00000x

www.rsc.org/

Aligned liquid crystal elastomers (LCEs) are capable of undergoing large reversible shape change in response to thermal stimuli and may act as actuators for many potential applications such as self-assembly and deployment of micro devices. Recent advances in LCE patterning tools have demonstrated sub-millimetre control of director orientation, enabling the preparation of materials with arbitrarily complex director fields. However, without design tools to connect the 2D director pattern with the activated 3D shape, LCE design relies on intuition and trial and error. Here we present a design methodology to generate reliable folding in monolithic LCEs designed with topology optimization. The distributions of order/disorder and director orientations are optimized so that the remotely actuated deformation closely matches a target deformation for origami folding. The optimal design exhibits a strategy to counteract the mechanical frustration that may lead to an undesirable deformation, such as anti-clastic bending. Multi-hinge networks were developed using insights from the optimal hinge designs and were demonstrated through the fabrication and reversible actuation of a self-folding box. Topology optimization provides an important step towards leveraging the opportunities afforded by LCE patterning into functional designs.

Introduction

Folding as a way to achieve controlled deformation has great potential as an integral part of engineering design such as self-assembly, deployment, and reconfigurable devices [1-5]. The art of origami uses fold operations to describe the transformation of a flat or curved surfaces into intricate 3D geometries. Of the many responsive material systems that have been investigated, reversible systems are particularly advantageous for deployable (foldable) origami-inspired devices as they may be utilized for reconfigurable devices that respond to changes in operating conditions. Accordingly, in device constructs such as antenna where form (shape) is a function, shape change is a vehicle to tuning a functional property. A recently introduced methodology for preparing complexly patterned liquid crystal elastomers (LCEs) [6] has been demonstrated to generate local, reversible strain fields with maximum strains of 55%. Heterogeneous in-plane director patterns and through-thickness strain profiles generate complex 3D shapes from an originally 2D LCE film upon thermal activation. However, only a small subset of the vast design space has been investigated due to a lack of predictive computational design tools. This article presents a topology optimization-based design method that utilizes the local control of nematic orientations to produce folding based target deformations.

Folds are important building blocks of origami designs, and their behavior largely influences the overall deformation. A simple valley fold (hinge) may be achieved by a localized through-thickness mismatch of expansion or contraction. Often this is obtained by layers of discrete strain response such as the bending observed in the common bimetallic strip. This approach has been used in a number of studies of self-folding systems [7-12]. The deformation in each system is governed by a complex combination of many factors including distribution of the strain, anisotropic material properties, shape and dimensions of the sample, distribution of the stimuli and hysteresis. Many of these techniques utilize multi-layered approaches to provide areas of locally reduced bending stiffness at the hinge. Folding in monolithic structures, without these local differences in bending stiffness, requires precise control of the folds to closely match a target shape.

Prediction of the deformation becomes increasingly challenging as the target becomes more complex. A fold in a context of origami, placed adjacent to other folds, may behave differently from the intended motion. For instance, mechanical multi-stability has been widely observed in folding of compliant materials. Bende et al. [13] exploited this behavior to introduce

snapping transitions in creased shells. In origami structures, Silverberg et al. [14] demonstrated that folds can be reversibly switched into a secondary stable state. By creating these folding defects, the mechanical properties of the structure can be widely tuned. In stimuli-responsive materials that exhibit complex shape changes, this multi-stability may lead to a number of different possible final configurations. Modes et al. [15] predicted a similar multiplicity of spatial configurations in a glassy liquid crystal network with twisted director orientations. This highly frustrated actuator led to a variety of possible bending modes. Each of these mechanisms can be attributed to deformations that are not localized to the fold. While this multi-stability is a potentially useful behavior for switching between spatial configurations, it can be deleterious when precise shape control is desired.

In this work, shape control is achieved by optimizing the LCE director pattern. Identifying the requisite director pattern for a specified shape remains an important LCE design challenge because of the complex relationship between the pattern and the predicted deformation. Our approach to addressing this challenge is to adopt topology optimization. Topology optimization is traditionally used in structural optimization to find optimal layouts of constituent materials and has also been applied in many emerging areas such as metamaterials, plasmonics, micro-fluidics and additive manufacturing [16-20]. An optimal topology is typically found by discretizing the design domain and optimizing an effective density assigned to each pixel. This is well suited to capture the flexibility afforded by the spatial control of photoalignment of LCEs. A density approach is used to find where to pattern, and director orientations are optimized to inform how to pattern, simultaneously. A numerical method is used to predict the deformation for a given design during the optimization process. Although high fidelity analysis methods incorporating elastodynamics and nonlinearity [21, 22] can predict deformations with better accuracy, their integration with design optimization is impractical due to their high computational costs. A low fidelity finite element analysis (FEA) with linear brick elements is used during the optimization. This not only reduces computational burden in each optimization iteration, but also reduces the complexity and cost of the sensitivity analysis. To verify the deformation in a large strain regime, beyond the limitation of linear analysis, the optimal design is analyzed with nonlinear FEA before fabrication and experiments.

The target shape for the LCE in this study is a hinge, which naturally integrates into the origami design motif. However, the formulation of the design tool is sufficiently general to address alternative criteria, such as strain energy, or target stress profiles. A target shape objective poses a design challenge at both micro and macro scales and its investigation offers insight on important aspects of design, modelling and material processing. In this article we describe the proposed design method and discuss the optimal hinge design found and its use in a self-folding origami box.

Design method

The objective of the design problem is to match the deformed LCE film to a hinge shape through the optimization of strain distribution. The recent report on the preparation of spatially patterned LCEs illustrated a use of twisted nematic alignment to introduce localized folding [6]. The twisted nematic orientation is a self-organized functionally graded orientation that naturally generates a local strain gradient through the thickness of the material along the primary (x'-) direction as seen in **Fig. 1.** However, this deformation is volume conserving and as such is accompanied by strains in the orthogonal directions, leading to anti-clastic bending as discussed in [11, 15]. In certain configurations, this curved fold can influence surrounding hinges to cause spontaneous "misfolding". An optimization problem is formulated to design a patterned LCE film that conforms to an ideal hinge shape on heating. Although a large fold angle at a high temperature is desirable in order to extrapolate the origami geometry towards closure, more emphasis is placed on controlling the shape in this formulation.

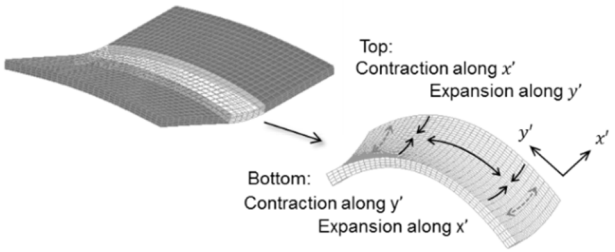

Fig. 1 A schematic of a twisted nematic hinge (left). An active area (center) is bounded by two inactive regions. The strains introduced in this sample on heating are shown (right).

The LCE patterning technique achieves control of the strain strength and orientation distribution through the photoalignment of the LCE within a small domain (pixel), specifying the local strain tensor. The alignment process can be chosen to skip some pixels, leaving them largely unresponsive to stimuli. The design of a patterned LCE film may be described through spatial distributions of separate control parameters that specify 1) strength, $S(x,y)$ and 2) orientation of the strain, $\phi(x,y)$. Strain strength is specified through the level of order, parameterized within each pixel i with an essentially binary control, i.e., polymers within each pixel i are considered either ordered ($S_i = 1$) or disordered, a lack of macroscopic orientation ($S_i = 0$), since the accuracy of adjusting the level of order to intermediate values is limited. Director orientations in ordered pixels may take any value in the range of $0 \leq \phi_i \leq 180°$ and may be distributed over the entire LCE film freely to achieve the optimal level of shape match. Using this photoalignment technique requires that director orientations be in the plane (tilt angle ~0), as such the design criteria were set to match this experimental limitation. Furthermore, the director orientation, as illustrated in **Fig. 2**, can vary hierarchically across the sample thickness. The director orientation through the thickness is

modelled by linearly interpolating values at the top and bottom surfaces as

$$\phi(x,y,z) = \phi(x,y,z_{bot}) + \frac{z}{z_{top} - z_{bot}}\Delta\phi(x,y) \quad (1)$$

where $\Delta\phi(x,y) = \phi(x,y,z_{top}) - \phi(x,y,z_{bot})$, and z_{top} and z_{top} are the z-coordinates of top and bottom surfaces. **Figure 2** illustrates an example of design control variables and the corresponding LCE pattern. It should be noted that this schematic depicts near perfect order, this system however has an orientational order parameter of ~0.5 [6].

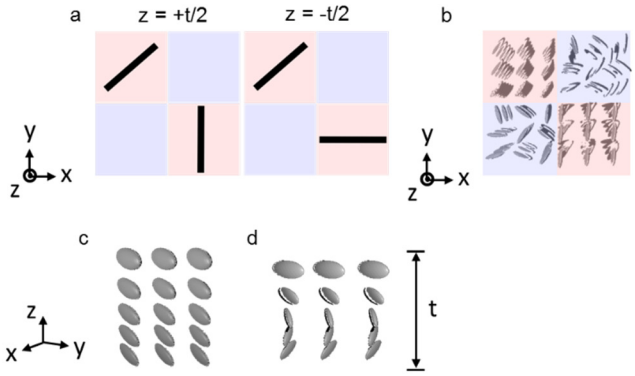

Fig. 2 Classification of the design domains and programmable director profiles a) Schematic of the design domain on top and bottom surface of the LCE. Design variables include the director orientation, ϕ (black line) and the color-coded order parameter, S_i. (order = red, disorder = blue). b) Representative 3D model of director ordering and orientation depicted in design domain schematic. Director orientations are assumed to be linearly interpolated through the thickness, t. Special cases include, c) planar domains, $\phi(z)$ = const. and d) twisted domain, $\phi(+t/2) = \phi(-t/2) + 90°$.

The numerical analysis of the deformation for a given strain distribution is carried out using FEA. The derivations of FE matrices are described in [23]. In short, the spontaneous strain tensor of a small domain of LCEs aligned along the reference orientation ($\phi = 0$) is modelled though the principal expansion coefficients α_x, α_y, α_z as functions of the actuation temperature T as

$$\boldsymbol{e_0} = \begin{bmatrix} \alpha_x(T) & 0 & 0 \\ 0 & \alpha_y(T) & 0 \\ 0 & 0 & \alpha_z(T) \end{bmatrix} \quad (2)$$

The spontaneous strain tensor in the rotated coordinate $\boldsymbol{e_0'}$ is computed as $\boldsymbol{e_0'} = \boldsymbol{L^T e_0 L}$ using the rotational transformation matrix

$$\boldsymbol{L} = \begin{bmatrix} cos\phi & sin\phi & 0 \\ -sin\phi & cos\phi & 0 \\ 0 & 0 & 1 \end{bmatrix} \quad (3)$$

The deformation is predicted through FEA using the spontaneous strain components corresponding to the actuation temperature, which may be read from strain vs. temperature data (see **Fig. S1)**. The level of order in each pixel is described by $0 \le S_i^p \le 1$ with a prescribed exponent p. Following the Solid Isotropic Material with Penalization (SIMP) method used in structural topology optimization [24], an exponent value $p > 1$ combined with a constraint on the fraction of patterned LCE area is used to facilitate convergence to solutions that are binary in $S(x,y)$. The engineering spontaneous strain components in the rotated coordinate can be expressed as

$$\boldsymbol{\varepsilon_0'} = \begin{bmatrix} \alpha_x S^p cos^2\phi + \alpha_y S^p sin^2\phi \\ \alpha_y S^p cos^2\phi + \alpha_x S^p sin^2\phi \\ \alpha_z S^p \\ 0 \\ 0 \\ 2(\alpha_x - \alpha_y) S^p cos\phi sin\phi \end{bmatrix} \quad (4)$$

The thickness of the sample is $t = 50\mu$m, and the expansion coefficients, Young's modulus, and Poisson's ratio are summarized in **Table 1**.

Table 1 LCE material parameters used in simulation

parameter	α_x	α_y	α_z	E	ν
value	-0.005	0.0025	0.0025	5MPa	0.49

The design optimization problem is to find optimal distributions of the order parameters and director orientations that minimize the deviation between the deformed film and the target shape, with a constraint on the ordered area fraction. The optimization problem is stated as follows.

$$\begin{aligned} &\text{Find } \boldsymbol{S}, \boldsymbol{\phi^{top}}, \boldsymbol{\phi^{bot}} \in \mathbb{R}^{\boldsymbol{N}} \text{ that} \\ &\text{Minimize} \quad f = (\boldsymbol{u} - \boldsymbol{u}^*)^T \boldsymbol{W} (\boldsymbol{u} - \boldsymbol{u}^*)/\widetilde{N} \\ &\text{Subject to} \quad g = \frac{\sum_i^N S_i}{N} - v_0 \le 0 \\ &\qquad 0 \le S_i \le 1 \;\forall\, i = 1,2,\cdots,N \\ &\qquad 0 \le \phi_i^{top} \le 180° \;\forall\, i = 1,2,\cdots,N \\ &\qquad 0 \le \phi_i^{bot} \le 180° \;\forall\, i = 1,2,\cdots,N \\ &\qquad \boldsymbol{Ku} = \boldsymbol{F} \end{aligned} \quad (5)$$

where N denotes the number of design pixels. The objective function is computed as a weighted sum of the displacements of the current design $\boldsymbol{u}$ and the target deformation $\boldsymbol{u}^*$, where $\boldsymbol{W}$ is a constant diagonal matrix specifying degrees of freedom (DOFs) included in the design consideration and $\widetilde{N}$ is the number of nonzero components in $\boldsymbol{W}$. The fraction of the ordered nematic area is constrained by v_0. As the number of design variables is large (25x25x3 = 1875 in the single hinge design example presented in this paper), a sensitivity analysis and a gradient based optimization algorithm are employed for their computational efficiency. A MATLAB routine developed by Svanberg [25] based on the method of moving asymptotes (MMA) is used, for its versatility in problems with many design variables.

The mechanical analysis for the design update is based upon an 8 node brick FE with linear elastic material behavior. The design domain consists of a 5mmx5mm specimen discretized into a 50x50 mesh with an order parameter and director orientation assigned to each element. The model assumes 1)

small displacement, 2) small strains (0.5%), 3) the spontaneous strain in disordered pixels is zero, and 4) the director orientation through the thickness changes linearly and can be adequately resolved by 4 brick layers. The linear analysis significantly reduces the computational cost of the optimization because the load step is not incremented and the stiffness matrix does not require updates. However, the small displacement assumption of the linear analysis focuses the optimization on finding the pattern needed to initiate folding and not necessarily the optimal solution for large folding.

Nonlinear mechanical analysis was employed to evaluate the folding performance of the predicted designs at larger strains (≥ 2.5%). The nonlinear analysis was performed in ANSYS 11.0 using 4 node shell elements with 4 layers. The director orientation profile from the optimal solution was assigned using the built-in element orientation angle ϕ, and was assigned for each element in a 50x50 mesh. The spontaneous strain of the LCE was assigned using the thermal expansion interface with anisotropic coefficients that were volume preserving. The shell element analysis accounted for geometric nonlinearity using an incremental thermal load step and an update of the stiffness matrix within a Newton Raphson iterative scheme.

After the computational analysis in both the small and large strain regimes, the order and director orientation profiles of the design are output to the patterning system for fabrication and tested via uniform heating. The design and experimental feedback process is outline in the flowchart of **Fig. 3**.

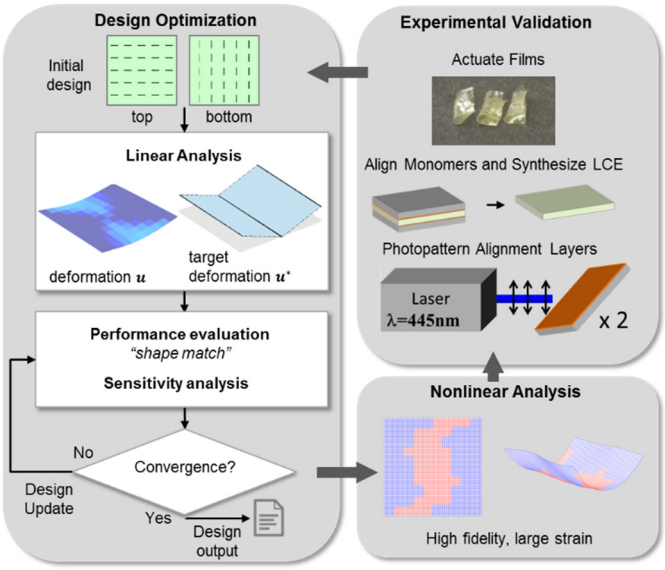

Fig. 3 Schematic of the design and fabrication feedback process. The deformation of a current design is predicted through linear analysis and compared with the target hinge shape. The optimization algorithm (MMA [25]) updates the design variables to reduce the deviation from the target deformation. The optimal solution is imported to ANSYS for verification through nonlinear analysis. A sample is fabricated using the LCE patterning technique [6] and heated to observe the self-actuated deformation.

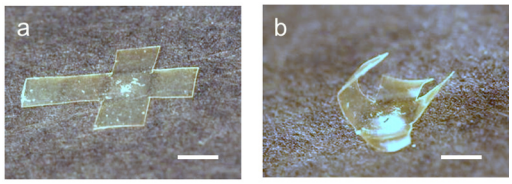

Fig. 4 Strain field incompatibilities between networked twisted nematic hinges inhibits collaborative folding. a) Box design patterned with 6 hinges in the flat, undeformed configuration (T = 23 °C). b) Deformed configuration of box after thermal activation (T = 150 °C). Competitive strains between hinges induce mis-folds along the short axis. Scale bar = 5mm.

Experimental method

The materials chemistry and optical patterning methodology introduced in [6] were employed to program the optimized director patterns predicted in this study. The localized patterns are written into alignment cells coated with a photoalignment layer by linearly polarized light over a 100μm x 100μm region corresponding to a design pixel with $S_i = 1$ to orient the LCE to the preferred direction specified by ϕ_i^{top}. The process is repeated for all of the elements $i = 1,2,\cdots,50^2$ and for the bottom layer using ϕ_i^{bot}. The cell is then assembled and filled with the nematic liquid crystal monomer mixture. The material aligns to the top and bottom alignment layers and takes on the programmed orientations. The composition and polymerization procedure used for the surface-aligning LCE has been reported elsewhere [6]. Briefly, a near stoichiometric mixture of a nematic diacrylate commonly referred to as RM82 (Merck) is mixed with *n*-butylamine and 1.5 wt% of a photoinitiator (I-369 Ciba). The nematic mixture is then filled into a previously patterned alignment cell and allowed to oligomerized at 75°C for 16 hours. After oligomerization, photopolymerization of the remaining acrylate groups traps the order of the designed pattern into an elastic solid. After crosslinking by photopolymerization the film is carefully removed from the glass cell. Actuation is performed using ambient heating. A non-adhesive surface, such as black paper, is placed onto a hot plate set at the desired temperature. A small temperature chamber is then assembled around the sample using glass slides. The system is allowed to equilibrate at each temperature for 5 minutes and then photographs are taken.

Results and discussions

An intuitive twisted nematic hinge discussed earlier can be modelled through a contraction along the fold direction at the top with $\phi = 0°$ and expansion at the bottom surface using $\phi = 90°$. Upon heating, the film creates a fold along the x'-direction, as illustrated in **Fig. 1**. However as the deformation is isochoric, the contraction is accompanied by expansion in the orthogonal directions within each pixel. In the plane of the sample this creates a competing deformation mode along the y-direction, creating an anticlastic, saddling shape [11, 15]. In our FE simulations, a significant saddling effect relative to the fold angle is observed during the initial deformation at small strain values

(see **Fig. S2**). Once the deformation goes beyond a certain strain level (~0.5%) saddling tapers off, as predicted in the nonlinear analysis. However, the linear analysis extrapolates this effect, predicting a significant saddling at large strains. The fold angle predicted by the linear analysis has a smaller rate of change, as brick elements are subject to shear locking at large strain values.

In experiments, twisted nematic hinges are folded in the predicted direction, however, the actuation of the adjacent folds acting on a shared compliant facet may result in a fold in the orthogonal direction. One such structure is the simple Latin cross with 5 hinges that is commonly used to make an origami box. On heating, the anti-clastic deformation of the four hinges connected to the central facet square influence each other. The result is the misfolding on the short arms of the cross. This is an example of an unwanted curvature at a micro-scale resulting in an undesirable shape at a macro-scale. In particular, the photograph in **Fig. 4** shows a network of twisted nematic hinges to create a box that has two facets experiencing the anti-clastic deformation caused by adjacent hinges. Our design optimization method is formulated, in part, in an attempt to overcome this undesirable outcome. Based on our observation from the linear and nonlinear analyses, controlling the initial deformation is critical in avoiding the anticlastic deformation, indicating that the design optimization process should focus on the small strain regime, at 0.5% maximum strain. Use of a small strain in the liner analysis during optimization also ensures the accuracy of the predicted deformation.

An optimal hinge design is found by solving the problem in Eq. (5), to match the deformed LCE film to a perfect hinge geometry shown in the insert of the flowchart in **Fig. 3** (see also **Fig. S3** for details). The deviation between the predicted and the target deformations are measured at nodes along the solid lines in **Fig. S3** and minimized. The centreline is selected, since enforcing the deformation of the hinge to be straight is critical for avoiding undesirable influences on adjacent facets and hinges. Facet edges are selected as target nodes, to specify the target fold angle. Shape control of the inner nodes along facets are less critical compared to the outline of the shape as they have no influence on adjacent components. The target fold angle, θ^* =2.5° is selected based upon the fold angle achievable using a twisted nematic hinge with a 20% active region. The small target fold angle reflects the small strain assumption in the analysis. The optimal solution is expected to produce a straight centreline, sacrificing the level of closure to some degree. Using the symmetry in the target shape, the number of design variables is reduced to a quarter of the number of elements representing different order and director properties. Parameters used in optimization are shown in **Table 2**, where S_{in}, ϕ_{in}^{top} and ϕ_{in}^{bot} represent the initial design variables used.

Table 2 Optimization parameters

parameter	N	v_0	p	S_{in}	ϕ_{in}^{top}	ϕ_{in}^{bot}
value	625	0.4	3	0.4	0	90°

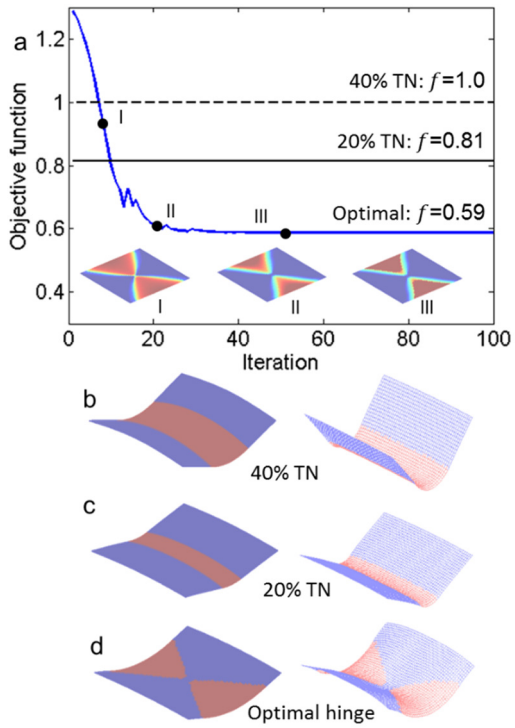

Fig. 5 Optimal pattern improves shape match over simple twisted nematic designs. a) Shape matching objective rapidly improved within the first 30 iterations. Inset: solution snap-shots at (I) 10, (II) 20, and (III) 50 iterations. Color represents the value of S_i (blue: S_i = 0, red: S_i = 1). Simulated deformed configurations for linear (left) and nonlinear (right) analyses for the b) wide (40%) twist nematic hinge, c) thin (20%) twist nematic hinge and d) thresholded optimal solution. Deformations shown in b)-d) are computed at a higher strain at 2.5% and exaggerated.

A smooth convergence leads to a significant performance improvement within the first 50 iterations as seen in **Fig. 5**a. A nearly binary solution for order parameter for each pixel S_i is obtained after additional 50 iterations. The objective function values of nematic hinges of two different aspect ratios (wide: 40%, thin: 20% active areas) are also reported for comparison. Each of the twisted nematic hinges has degraded performance in terms of the specified objective function, mainly due to the saddling along the hinge.

The optimal order/disorder pattern and director orientation distribution are shown in **Fig. 6**c along with those of the twist nematic hinges (**Fig. 6**ab). Comparison of the director orientation distributions reveals that the optimal design achieves folding through a similar mechanism as the twisted nematic hinges: contraction in the $\phi = 0°$ direction at the top and expansion in the $\phi = 90°$ direction at the bottom surface, to create a strain gradient through thickness. However, triangular distributions of active areas, instead of rectangular regions, are observed with slanted director orientations at the edges of triangular regions. These features somewhat resemble parts of a +1 topological defect. The top layer is a segmented +1 azimuthal disclination with continually rotating director orientations creating circular profiles with a singularity at the center; the bottom layer is a

segmented +1 radial disclination. The orientation of the director rotates 90° through the thickness of the film from radial to azimuthal, creating a pattern called "radimuthal" presented in [15, 26]. In the optimal hinge design, the distribution of inactive regions leads to a removal of saddling by reducing the strain near the center, and re-distribution of active regions towards the outer edges helps to evoke the desired, folding motion.

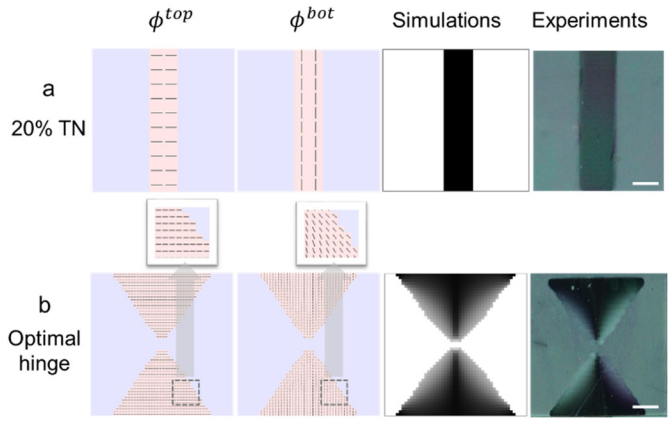

Fig. 6 Through-thickness director orientation is successfully patterned. Schematics of top, ϕ^{top}, and bottom, ϕ^{bot}, surface director profiles and a color-coded plot indicating the director orientations for the a) 20% twisted nematic and b) optimal hinge design. Images of each hinge under cross-polarizing lenses confirms the ϕ distributions were successfully programmed. Scale bar = 1mm.

The single hinge designs were experimentally patterned and the resulting films were actuated and characterized a minimum of 3 times. On heating the 40% twisted nematic hinge folds from flat to 89°. On cooling to room temperature, the hinge largely unfolds, but a residual angle of 15° remains. The optimized hinge folds from flat to 85°. On cooling a residual angle of 9° is observed. This retained deformation can be attributed to residual strain in the sample, which is more readily observed in the twisted nematic samples. The deformation is largely reversible after the initial cycle. The slight distortion of the square facets observed in **Fig. 7**a, may be a result of anisotropic contractions in the un-patterned regions indicating a violation of our assumption of non-responsiveness in the disordered regions. Mechanical performance is summarized in the fold angle vs. temperature plot of **Fig. 7**b. The plot illustrates a monotonic increase of the fold angle in all hinge designs. Although the fold angle attainable in the optimal hinge at the strain level used during optimization is small, the fold angle extrapolates towards closure ($\theta = 90°$) with higher strain values at higher temperatures. The rate of increase of the fold angle is higher in twisted nematic hinges by ~6%. This indicates that a desired level of closure can be achieved by adjusting the temperature, with a slightly higher sensitivity in twisted nematic hinges. The more important performance evaluation, however, is in the deformation control of networked hinges. As illustrated in **Fig. 4**b, the twisted nematic hinge led to a misfold due to saddling. The reduction of the mechanical frustration in the optimal hinge indicates that an origami box made with networked optimal hinges may lead to an improved deformation.

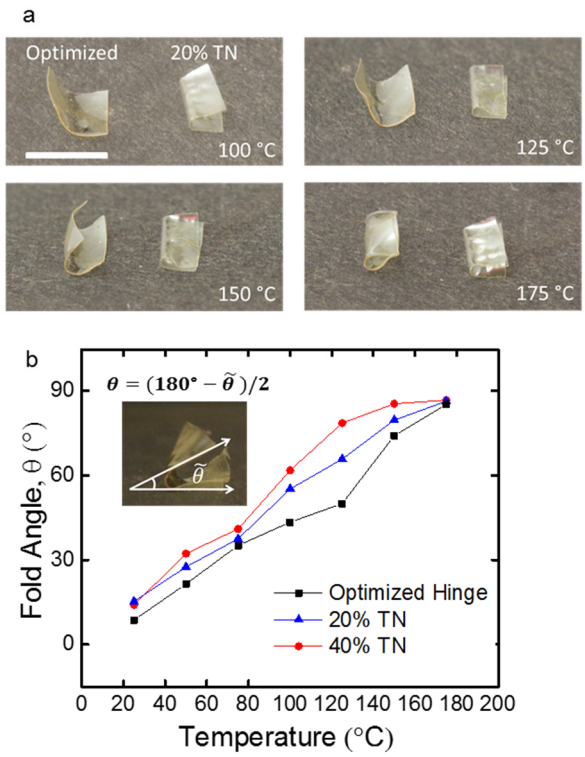

Fig. 7 Fold angle attainable through various hinge designs. All hinges achieve a monotonic increase in fold angle with increased temperature towards closure ($\theta = 90°$). a) Representative images of the optimal hinge and 20% twisted nematic hinge at different temperatures. Scale bar = 5mm. b) Fold angle vs temp curves. Inset: schematic of fold angle definition.

A box design inspired by the optimal hinge is shown in **Fig. 8**d. Four smoothed optimal hinges are patterned at the base of each flap and networked through a rotation and superposition of the overlapped director profiles. The director orientation is rotated by 90° through thickness. Again, the design resembles a discrete approximation of a radimuthal pattern around each corner of the box base but with a quarter of the pattern cut off. The image of the fabricated LCE film under a cross-polarizer is shown in **Fig. 8**f. Upon heating the film undergoes a desired deformation with all four flaps folding up, creating a box (see **Fig. 8**g).

The fabricated box pattern in **Fig. 8**f exhibits multi-stability with deformation modes other than a box shape in nearby energy levels, which may be accessed by applying forces near hinges. Depending on the sample preparation and actuation conditions, the deformation may be steered into an undesirable mode. Potential contributing factors to this discrepancy include some level of order in un-patterned regions, the effect of domain interfaces, temperature distribution, elastodynamic effect and anisotropy of the constituent material. Although these issues are not addressed in our current model, use of the initial deformation in the design process was effective in alleviating the mechanical

frustration of the hinge network and improved the likelihood of folding in the desired direction.

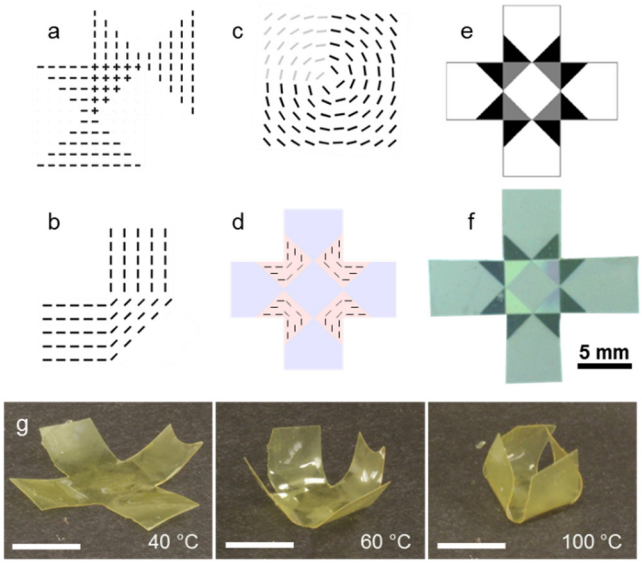

Fig. 8 Multi-hinge network solution inspired by the optimal hinge design. a) Optimal hinges are assembled into a multi-hinge network through a rotation and superposition of the overlapped director angles. b) Top surface director profile of corner joint connecting two hinges. c) The hinge joint resembles a discrete form of a +1 topological defect. d) Order level and director orientation profiles of a box on the top layer. e) Diagram of color-coded director orientations ϕ. f) Image of box pattern under cross-polarizing lenses. g) Images of LCE box at different temperatures demonstrating thermal control of actuation. Full closure achieved at 100 °C.

Conclusions

A topology optimization method is used to determine an optimal director profile to prepare hinges in an LCE that undergo clastic rather than anti-clastic deformation. The optimal hinge design exhibits triangular regions of order and director orientation distributions similar to a radimuthal +1 defect, without assuming the prior knowledge of this intricate pattern. The director orientations twist through the thickness of the material to achieve large out-of-plane deformation, and the pattern makes use of inactive regions in order to counteract the anti-clastic deformation seen in previously reported twisted nematic hinges. A novel box design inspired by the optimal hinge design is predicted, prepared, and characterized. The design method introduced in this work efficiently explores a large design space for specific design objectives, presenting a step toward leveraging the engineering potential of the programmable anisotropy and heterogeneity of LCEs.

Based on our trials of design and experiments, some of the material assumptions in the model deviated from the experimental observations such as the multi-stability in patterned films and the undesired deformation in polydomain. Incorporation of these effects into the model would improve the predictability of complex deformation and repeatability in experiments but at a higher computational cost. Determination of the appropriate treatment of these complex phenomena is dependent on the level of accuracy required by the design process. For the target shape objective used in this study, the level of model detail was sufficient. In addition, the design process may be modified to alleviate computational burden and undesirable material behaviors for complex target shapes. Potential modification currently under investigation include aggressive use of enforced symmetry in optimal design, implementation of design filters for smooth director orientation transitions and parallelization of the FEM computation.

This work demonstrates the value of using a new material processing technique in conjunction with design optimization. Formulation of a design optimization problem requires us to clearly define evaluation metrics relevant to functions. This is an important step towards leveraging advances in material processing techniques into functional designs.

Acknowledgements

This research is supported by the Air Force Office of Scientific Research (AFOSR) funding, LRIR 13RQ02COR.

This work was supported in part by an allocation of computing time from the Ohio Supercomputer Center.

THW and TJW would like to thank J.J. Wie for helpful discussions.

Notes

* These authors contributed equally to this work.

+ Corresponding author.

[a] Aerospace Systems Directorate, Air Force Research Laboratory, Wright-Patterson AFB, OH 45433-7531, USA.

[b] Material and Manufacturing Directorate, Air Force Research Laboratory, Wright-Patterson AFB, Ohio 45433-7750, USA.

[c] Wright State Research Institute, Beavercreek, OH 45431, USA.

[d] Azimuth Corporation, Beavercreek, OH 45431, USA.

[e] Present address: Department of Bioengineering, The University of Texas at Dallas, Richardson, TX 75080-3021, USA.

Electronic Supplementary Information (ESI) available: see attached.

References

1. D. H. Gracias, V. Kavthekar, J. C. Love, K. E. Paul and G. M. Whitesides, *Advanced Materials*, 2002, **14**, 235.
2. L. A. Bowen, C. L. Grames, S. P. Magleby, L. L. Howell and R. J. Lang, *Journal of Mechanical Design*, 2013, **135**, 111008.
3. S. Felton, M. Tolley, E. Demaine, D. Rus and R. Wood, *Science*, 2014, **345**, 644-646.
4. K. Kuribayashi-Shigetomi, H. Onoe and S. Takeuchi, *PloS one*, 2012, **7**, e51085.
5. K. Kuribayashi, K. Tsuchiya, Z. You, D. Tomus, M. Umemoto, T. Ito and M. Sasaki, *Materials Science and Engineering: A*, 2006, **419**, 131-137.
6. T. H. Ware, M. E. McConney, J. J. Wie, V. P. Tondiglia and T. J. White, *Science*, 2015, **347**, 982-984.
7. E. A. Peraza-Hernandez, D. J. Hartl, R. J. Malak Jr and D. C. Lagoudas, *Smart Materials and Structures*, 2014, **23**, 094001.
8. J. H. Na, A. A. Evans, J. Bae, M. C. Chiappelli, C. D. Santangelo, R. J. Lang, T. C. Hull and R. C. Hayward, *Advanced Materials*, 2015, **27**, 79-85.
9. Y. Liu, J. K. Boyles, J. Genzer and M. D. Dickey, *Soft Matter*, 2012, **8**, 1764-1769.
10. C. Liu, H. Qin and P. Mather, *Journal of Materials Chemistry*, 2007, **17**, 1543-1558.
11. L. T. de Haan, A. P. Schenning and D. J. Broer, *Polymer*, 2014, **55**, 5885-5896.
12. J. Ryu, M. D'Amato, X. Cui, K. N. Long, H. J. Qi and M. L. Dunn, *Applied Physics Letters*, 2012, **100**, 161908.

13. N. P. Bende, A. A. Evans, S. Innes-Gold, L. A. Marin, I. Cohen, R. C. Hayward and C. D. Santangelo, *arXiv preprint arXiv:1410.7038*, 2014.
14. J. L. Silverberg, A. A. Evans, L. McLeod, R. C. Hayward, T. Hull, C. D. Santangelo and I. Cohen, *science*, 2014, **345**, 647-650.
15. C. Modes, M. Warner, C. Sánchez-Somolinos, L. De Haan and D. Broer, *Physical Review E*, 2012, **86**, 060701.
16. M. P. Bendsoe and O. Sigmund, *Topology optimization: theory, methods and applications*, Springer Science & Business Media, 2003.
17. A. R. Diaz and O. Sigmund, *Structural and Multidisciplinary Optimization*, 2010, **41**, 163-177.
18. J. Andkjær, S. Nishiwaki, T. Nomura and O. Sigmund, *JOSA B*, 2010, **27**, 1828-1832.
19. S. Kreissl, G. Pingen, A. Evgrafov and K. Maute, *Structural and Multidisciplinary Optimization*, 2010, **42**, 495-516.
20. D. Brackett, I. Ashcroft and R. Hague, 2011.
21. L. T. de Haan, V. Gimenez-Pinto, A. Konya, T. S. Nguyen, J. Verjans, C. Sánchez-Somolinos, J. V. Selinger, R. L. Selinger, D. J. Broer and A. P. Schenning, *Advanced Functional Materials*, 2014, **24**, 1251-1258.
22. V. K. G. Pinto, Kent State University, 2014.
23. K. Fuchi, P. R. Buskohl, T. Ware, R. A. Vaia, T. J. White, G. W. Reich and J. J. Joo, 2014.
24. M. P. Bendsøe and O. Sigmund, *Archive of applied mechanics*, 1999, **69**, 635-654.
25. K. Svanberg, *International journal for numerical methods in engineering*, 1987, **24**, 359-373.
26. L. T. de Haan, C. Sánchez-Somolinos, C. M. Bastiaansen, A. P. Schenning and D. J. Broer, *Angewandte Chemie International Edition*, 2012, **51**, 12469-12472.

Table of Contents Entry

SoftMatter

Title: Topology Optimization for the Design of Folding Liquid Crystal Elastomer Actuators

Kazuko Fuchi*, Taylor H. Ware*, Philip R. Buskohl, Gregory W. Reich, Richard A. Vaia, Timothy J. White and James J. Joo

Graphic

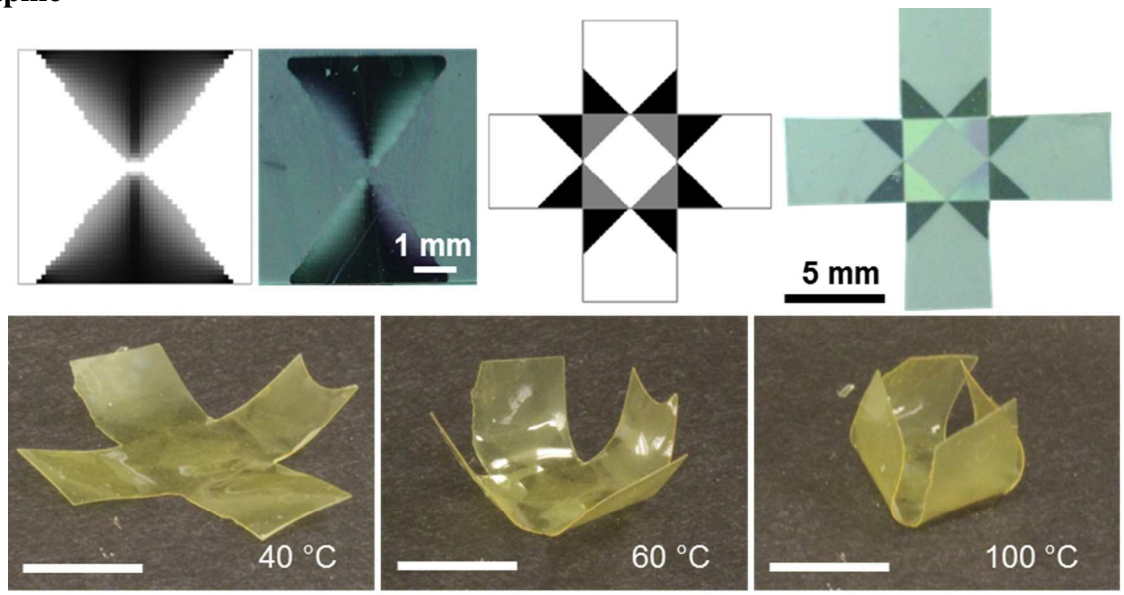

Summary

A topology optimization method is used to take advantage of programmable anisotropy in LCE to achieve target deformations.